



Removal of ciprofloxacin from aqueous solution by a three-dimensional electrocoagulation process using $\text{Fe}_3\text{O}_4@\text{AC}$ nanocomposite as a particle electrode in combination with persulfate: nonlinear fitting of isotherms and kinetic models

Mohammad Ahmadian^{a,b}, Mohammad Malakootian^{a,b,*}, Majid Aghasi^b, Ali Fatehizadeh^{c,d}

^aEnvironmental Health Engineering Research Center, Kerman University of Medical Sciences, Kerman, Iran, Tel. +98 34 31325856; Fax: +98 34 31325856; emails: m_malakootian@kmu.ac.ir (M. Malakootian); m_ahmadi@kmu.ac.ir (M. Ahmadian)

^bDepartment of Environmental Health, School of Public Health, Kerman University of Medical Sciences, Kerman, Iran, email: maghasi@kmu.ac.ir (M. Aghasi)

^cEnvironment Research Center, Research Institute for Primordial Prevention of Non-communicable Disease, Isfahan University of Medical Sciences, Isfahan, Iran, email: fatehizadeh@gmail.com (A. Fatehizadeh)

^dDepartment of Environmental Health Engineering, School of Health, Isfahan University of Medical Sciences, Isfahan, Iran

Received 12 January 2020; Accepted 3 June 2020

ABSTRACT

In the present study, the removal of ciprofloxacin (CIP) from aqueous solutions was performed using the magnetic $\text{Fe}_3\text{O}_4@\text{AC}$ (MAC) nanocomposite as a particle electrode in three-dimensional electrocoagulation (EC) system, as well as using persulfate (PS) to increase the removal efficiency. First, the MAC nanocomposite was synthesized and then characterized by X-ray diffraction, vibrating-sample magnetometer and field emission scanning electron microscopy, energy-dispersive X-ray spectroscopy, Mapping and Fourier-transform infrared spectroscopy analyses. Each process was evaluated separately and the appropriate process was selected. The results confirmed the spherical structure of the MAC nanocomposite, with the smallest amount of clogging, uniform distribution of the elements on the nanoparticle surface and the creation of suitable magnetic properties. The CIP removal values for each of PS, EC, MAC, EC-MAC and EC-MAC-PS processes were 0%, 0%, 70%, 94.2% and 98.9%, respectively. However, since significant amounts of non-recoverable sludge were formed in the EC-MAC-PS process, no sludge was produced in the EC-MAC process, and only recoverable nanoparticles existed, PS was excluded from the tests. Finally, optimal conditions for the EC-MAC process were determined. Under the optimum conditions: CIP (10 mg/L), MAC (0.9 g/L), pH (7), current density (0.3 mA/cm²) and contact time (35 min) the CIP removal efficiency was 98.21%. The results revealed that the Avrami fractionary and pseudo-second-order kinetic models fitted better the experimental results and Q_{max} of MAC nanocomposite obtained from the Langmuir isotherm model was 97.39 mg/g. Based on the results, the EC-MAC process has a good efficiency in removing the CIP antibiotic and can be considered as an economical process.

Keywords: Ciprofloxacin; Electrocoagulation; $\text{Fe}_3\text{O}_4@\text{AC}$; Nanocomposite; Three-dimensional

* Corresponding author.

1. Introduction

Contamination of water resources in today's world has become a serious problem and many pollutants have been discharged into the environment through a variety of industrial, agricultural and other activities. Antibiotics are a new class of emerging pollutants produced and used for therapeutic purposes for humans and animals. Besides, large quantities of these compounds are being used in agricultural activities [1,2]. Antibiotics, because of their chemical structure, fall into the category of substances that are called highly non-degradable and are not degraded by conventional methods utilized to treat hospital wastewaters. As a result, large amounts of them are released into the environment without sufficient treatment, which can contaminate water resources [3,4]. Even small contents of antibiotics can increase the population of resistant bacteria in the future, which makes antibiotics unable to cure infections. These pollutants also have a cyclic structure and cause various health effects, including mutagenicity and carcinogenicity [5,6]. Ciprofloxacin (CIP) is one of the most important antibiotics belonging to the fluoroquinolone family; it is widely used to treat human and animal infections [7,8]. The presence of CIP in drinking water may cause various side effects on humans such as diarrhea, nausea, vomiting, tremor, headache and nervousness and interference with plant photosynthesis and apparent deformation in plants [9–11]. As mentioned, conventional biological treatment methods cannot remove antibiotics; thus, new processes should be developed to eliminate them. Many methods have recently been used to remove CIP from aqueous solutions such as reverse osmosis [12], membrane ultrafiltration [13], membrane bioreactors [14], adsorption [15], and so forth. Advanced oxidation processes are new methods for wastewater treatment and the electrochemical technique is one of them, which has been utilized in many researches due to its high efficiency, versatility and environmental friendliness [16,17]. Among electrochemical methods, the utilization of three-dimensional (3D) electrodes has been taken into account by various researchers; these new systems are on the basis of traditional two-dimensional (2D) electrode devices filled with some conductive particles that are called particle electrodes [18,19]. In 3D-electrocoagulation (EC), after electric current generation, the particles are subjected to electrostatically induced polarization to form numerous microelectrodes, which can not only increase the specific electrode surface but also shorten the migration distance of the pollutants, leading to an improvement in process efficiency and capacity [20–22]. Compared to the 2D electrodes, the 3D-based electrode system, under similar conditions, has higher degradation efficiency, lower energy consumption, shorter reaction time and less sludge production. Moreover, the microelectrodes are recyclable and reusable, which overall reduce costs compared to other electrochemical processes [23–26]. Among strong oxidizers, persulfate (PS) and its sulfate radical have unique properties, such as higher kinetic speed, greater stability than hydroxyl radicals and are less influenced by natural organic matters. Combining PS with EC can activate PS using the electrons produced in the cathode according to Eq. (1). Also, based on Eq. (2), PS is regenerated in the anode, which results in the production

of a continuous cycle of radical sulfate and PS production, which causes an increase in process efficiency [1,27].



Therefore, the purpose of the present study was to use the 3D-EC using the magnetic $\text{Fe}_3\text{O}_4@\text{AC}$ (MAC) nanocomposite in combination with sulfate radicals.

2. Materials and methods

2.1. Materials and devices

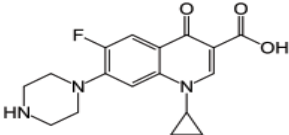
All the chemicals used in this study were of analytical grade. Chemical materials including NaOH, HCl, NaCl, $\text{FeCl}_3 \cdot 6\text{H}_2\text{O}$, $\text{FeCl}_2 \cdot 4\text{H}_2\text{O}$, NH_4^+ , sodium PS and powdered activated carbon (PAC) were purchased from Merck (Germany). CIP (purity $\geq 98\%$) was procured from Temad Pharmaceutical Company (Tehran, Iran). The properties of CIP have been shown in Table 1.

Deionized water was used to provide the necessary solutions. Since the antibiotic half-life of CIP is about 5.5 h, the synthetic solutions were made daily before the experiments began. Also, pH meter (HANNA, USA), DC power supply (Pars Azma, Iran), scales (Sartorius, Germany), magnetic stirrer (Heidolph, Germany), spectrophotometer (Shimadzu, Japan) and atomic absorption device (Shimadzu, Japan) were used during the tests.

2.2. Synthesis of MAC nanocomposite

To synthesize the MAC nanocomposite, the PAC was first placed at 550°C for 2 h to eliminate potential organic impurities. Next, PAC (2 g), $\text{FeCl}_3 \cdot 6\text{H}_2\text{O}$ (2 mmol) and $\text{FeCl}_2 \cdot 4\text{H}_2\text{O}$ (1 mmol) were added to 100 ml of deionized water. The mixture was then inserted into a 250 ml beaker and placed on a magnetic stirrer with a hot plate. A burette containing ammonia solution and a thermometer were fixed on the surface of the beaker. The thermometer was inserted into the solution and, as the beaker contents were being stirred, the temperature of the solution was fixed using a heater at 60°C – 70°C . After the temperature was fixed, the

Table 1
Properties of CIP

Drug class	Fluoroquinolone
Chemical formula	$\text{C}_{17}\text{H}_{18}\text{FN}_3\text{O}_3$
Molar mass	331.346 g/mol
K_{ow}	1.9
Solubility	Soluble in 0.1 N HCl at 25 mg/mL
Chemical structure	

ammonia solution was slowly added and the pH value was checked every 5 min using pH paper. The addition of ammonia continued until the pH reached about 11 and was subsequently checked by a magnet for magnetization. After ensuring the magnetic properties, the synthesized nanocomposites were washed several times using deionized water until the pH reached a neutral limit. Finally, the nanocomposites were dried at 60°C for 24 h.

2.3. MAC nanocomposite characterizations

After synthesizing the MAC nanocomposite, its properties were determined by field emission scanning electron microscopy (FESEM), energy-dispersive X-ray spectroscopy (EDS), mapping (TESCAN MIRA3, Czech Republic), X-ray diffraction (XRD) (PANalytical, Netherlands), vibrating-sample magnetometer (VSM 7400 M, USA), and Fourier-transform infrared spectroscopy (FTIR 27 Tensor) analyses. One sample of the nanocomposite was analyzed by FTIR, XRD and EDS after the EC-MAC process. Furthermore, one sample of the produced sludge was sent to the EDS analysis after the EC-MAC-NaCl and EC-MAC-PS processes.

2.4. Pilot specification

In this study, a 700 ml cylindrical reactor capable of containing 500 ml solution was utilized. Two brass electrodes (40% zinc and 60% copper) were used as the cathode and anode, respectively. The dimensions of the electrodes were 40 mm × 120 mm × 1 mm that were connected to a DC power supply and separated by 4 cm apart. A magnetic stirrer and magnet were used to mix the contents of the reactor. Fig. 1 shows an overview of the pilot used in the present study.

2.5. Experimental set up

2.5.1. Effect of EC, PS, MAC, EC-MAC, EC-MAC-NaCl and EC-MAC-PS

At the beginning of the experiments, each of the EC, PS, MAC, EC-MAC, EC-MAC-NaCl, EC-MAC-PS processes were evaluated separately. To this end, solutions containing initial CIP concentration of 20 mg/L were prepared and their pH was adjusted to 5. Then, the experiments were

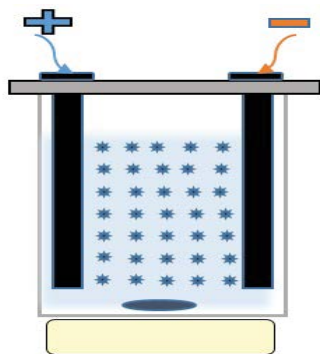


Fig. 1. A schematic diagram of the pilot used in the study.

performed under the following conditions: EC = 1 mA/cm², PS = 300 mg/L, MAC = 0.9 g/L and NaCl = 0.5 g/L.

2.5.2. Effect of key parameters on EC-MAC

The EC-MAC process at different pH values (3, 5, 7 and 9), initial CIP concentrations (10, 20, 30 and 40 mg/L), different MAC concentrations (0.3, 0.6 and 0.9 g/L) and different current density (CD) values (0.3, 0.6, 1 and 1.32 mA/cm²) were carried out.

2.6. Analysis

To determine the solubility of the electrodes during the EC-MAC process, the effluent and sludge were sampled. The effluent sample was analyzed by atomic absorption for determination of copper and zinc contents and the sludge sample was also sent for the EDS analysis. During the experiments, the reactor was sampled once every 5 min and the residual CIP values at $\lambda_{\max} = 276$ nm were determined using a spectrophotometer (Shimadzu's UV-1800 UV-VIS, Japan). The residual amount of CIP (RE) was determined by Eq. (3).

$$RE = \frac{CIP_0 - CIP}{CIP_0} \times 100 \quad (3)$$

CIP₀: initial CIP concentration (mg/L); CIP: final CIP concentration (mg/L).

3. Results and discussion

3.1. Characterization of MAC nanocomposite

The results of the FESEM analysis have been shown in Figs. 2a and b. As can be seen, the nanoparticles were almost spherical with the smallest amount of clogging at 31–28 nm. The results of the mapping analysis shown in Fig. 2c also confirm the uniform distribution of iron, carbon and oxygen elements on the MAC nanocomposite surface. According to the EDS analysis (Fig. 2d) for the MAC nanocomposite, iron, carbon and oxygen elements with expected values of C (31.04%), Fe (24.34%) and O (44.61%) were observed.

The results of the FTIR analysis for the MAC nanocomposites have been shown in Fig. 3a. As shown in FTIR spectra, the absorption band observed at 582 cm⁻¹ is related to the tensile vibrations of metal-oxide (Fe–O) in the Fe₃O₄ compound present in the MAC nanocomposite structure. The absorption band observed at 3,430 cm⁻¹ is related to the OH groups due to the moisture absorbed on the surface of the MAC nanocomposite. Also, according to the XRD analysis (Figs. 3b and c), the magnetite (Ref. Code: 96-900-5840) and graphite (Ref. Code: 96-901-2706) phases were identified; thus, in the MAC structure, both phases were identifiable. The peak at 2θ values of 26.61° related to carbon and the peaks at 2θ values of 18.47%, 29.5%, 30.27%, 35.64%, 43.26%, 53.66%, 57.21%, 62.82%, 71.38% and 74.31% related to Fe₃O₄ are visible in the MAC nanocomposite structure. Fig. 3d also shows the results of the VSM analysis with respect to the magnetic saturation (Ms) obtained at about 36 emu/g; this confirms

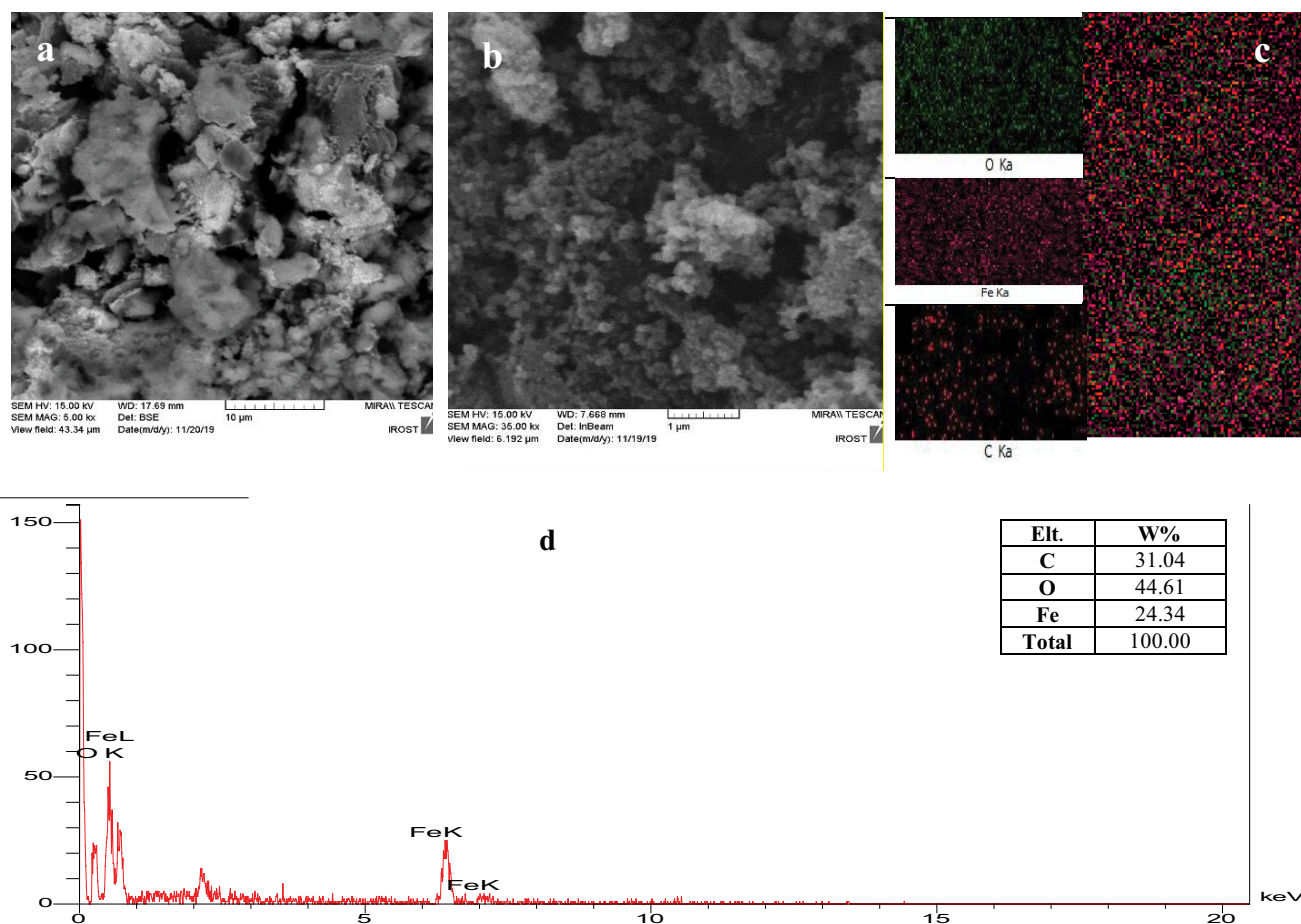


Fig. 2. Results of (a and b) FESEM, (c) mapping, and (d) EDS for the characterization of the MAC nanocomposite.

the high magnetic strength of the MAC nanocomposite, which provides its separation from the aqueous solution.

3.2. Comparison of EC, PS, MAC, EC-MAC, EC-MAC-NaCl and EC-MAC-PS

In this study, the performance of each process and combined processes were evaluated. Fig. 4 shows the results of each of the EC, PS, MAC, EC-MAC, EC-MAC-NaCl and EC-MAC-PS methods. As shown, the EC process alone after 60 min of contact time had no effect on CIP removal. In 3D-EC, electrodes including anode, cathode and particle electrodes are one of the most important determinants. In the conventional EC process, iron and aluminum electrodes are usually used. But, when iron or aluminum electrodes are used as the anode in 3D-EC, anodic corrosion causes the release of iron and aluminum and, in turn, metal hydroxide clots are formed [1]. The formation of these clots in 3D-EC is undesirable because they are adsorbed on the particle electrodes and, in turn, reduce the efficiency of the 3D systems [28]. The most common types of electrodes used in anode in 3D-EC systems include platinum, titanium, and boron-doped diamond, all of which are very expensive [26,29,30]. Therefore, in this study, a relatively inexpensive and available brass metal was used in the 3D-EC system. As noted,

the EC process using brass electrodes had no effect on the removal of the CIP antibiotic; this can be due to the lack of the flocculation property of the copper and zinc metals present in the electrode composition. The resistant structure of the CIP antibiotic is another reason for this phenomenon [2,8]. As shown in Fig. 4, the PS process alone had no effect on the removal of CIP owing to the absence of an activator. Since PS is a non-selective, soluble anion that is relatively stable at room temperature and is the strongest oxidant of the peroxymen family under atmospheric conditions, it has little effect on the removal of organic pollutants. However, if heat, light or metal ions and magnetic nanoparticles are used as a catalyst, the reaction of PS enhances dramatically and increases the production of sulfate radicals [27,31–33]. In the study by Cai et al., in which photoexcited dye was used to activate PS for tetracycline removal, minor amounts of the antibiotic were removed when PS was applied separately; this observation accords with the results of the present study [34]. Also, similar results were reported in the study by Malakootian et al. [1], who used the EC-PS process to remove CIP from aqueous solution.

In the process by means of using the MAC nanocomposites alone after 60 min contact time, 70% of CIP was removed. The phenomenon is also due to the adsorption of antibiotics onto the high surface area of magnetic carbon,

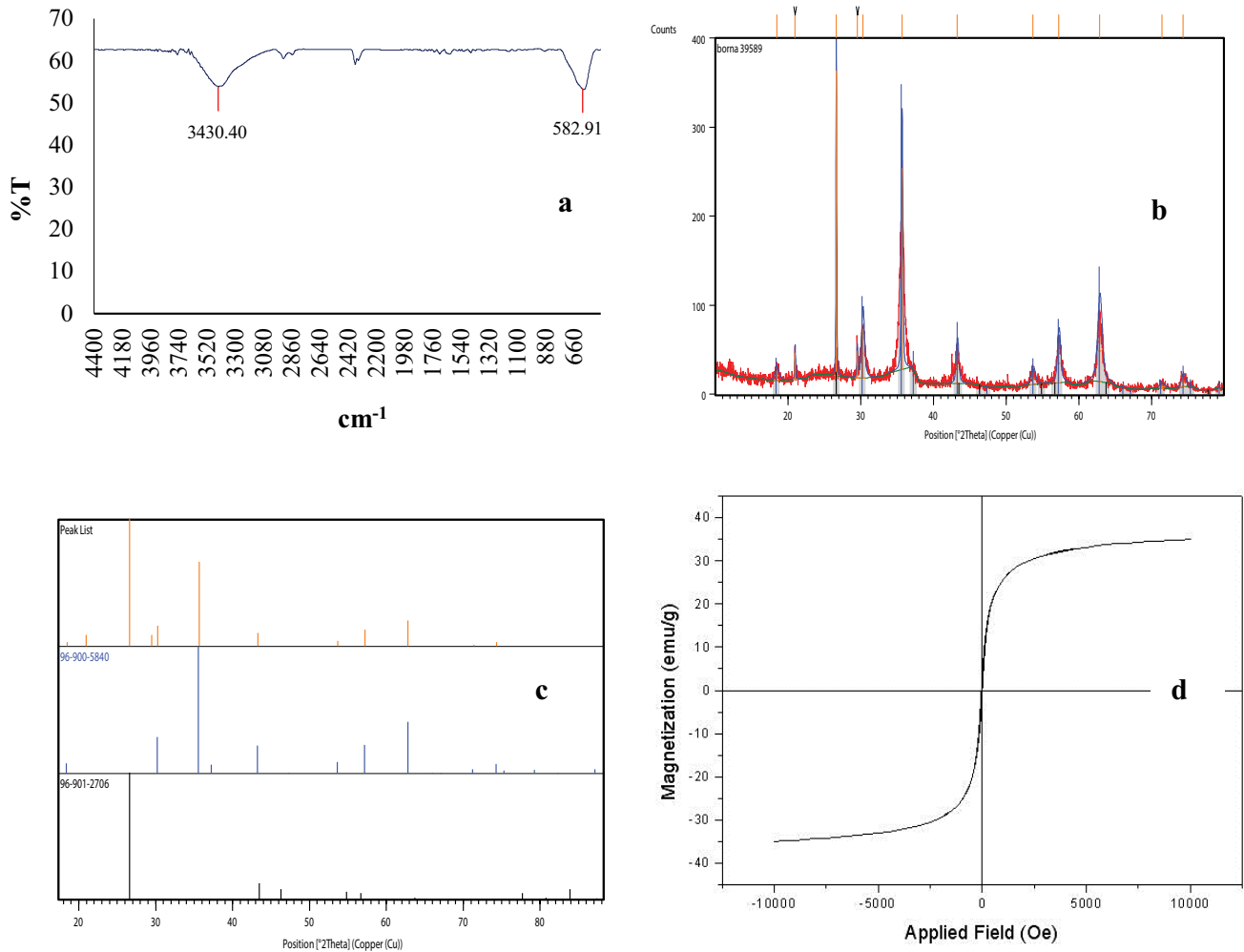


Fig. 3. Results of (a) FTIR, (b and c) XRD, (d) VSM analyses for the MAC nanocomposite.

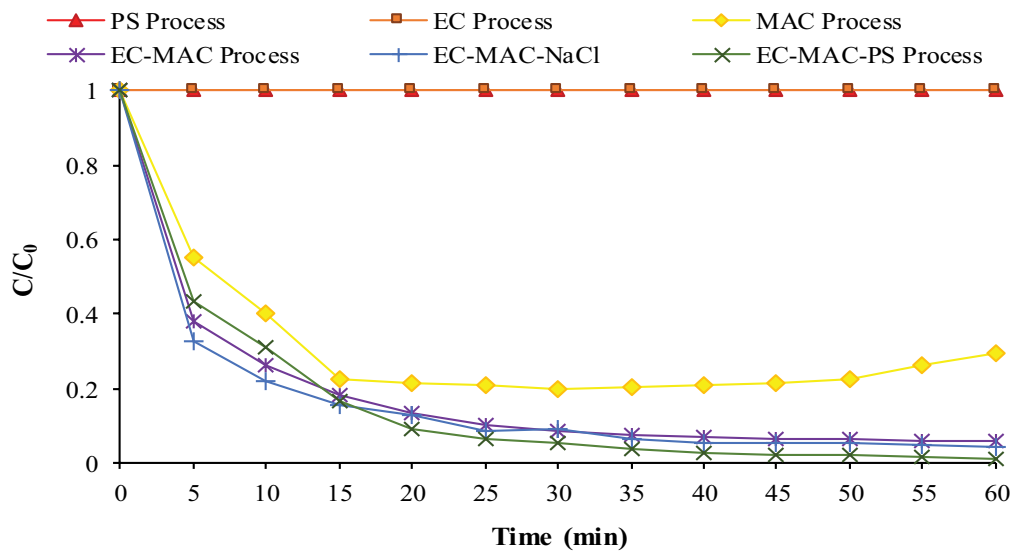


Fig. 4. The effect of EC, PS, MAC, EC-MAC, EC-MAC-NaCl and EC-MAC-PS on CIP removal (EC = 1 mA/cm², PS = 300 mg/L, MAC = 0.9 g/L, contact time = 60 min and NaCl = 0.5 g/L).

the chemistry of adsorbent surface such as the presence of surface groups and the presence of functional groups that cause the antibiotic to separate from the solution and sit on the adsorbent surface [6,10,15,35,36]. In the study by Gupta and Garg, who used granular activated carbon (GAC) to remove CIP, the performance was about 65% after a long contact time (7 h). In the study by Darweesh and Ahmed [38], who applied activated carbon in the columnar mode for CIP removal, they reported a similar efficiency at the same contact time.

The EC-MAC process eliminated 94.5% of CIP after 60 min, with a 25% increase in CIP removal efficiency compared to the MAC process alone, which could be further enhanced by optimizing the test conditions. In fact, during this process, the MAC nanocomposites play a role as the particle electrodes. These electrodes have both positive and negative charges when they are placed in an external magnetic field. As a result, charged pollutants in the magnetic field move to a part of the particle electrode with the opposite charge. This phenomenon was called the electro-sorption that occurs during the 3D-EC process. In 3D-EC, pollutants are also eliminated by electrochemical oxidation resulting from the hydrolysis of water and the formation of hydroxyl radicals. As a result, the combination of the electrochemical oxidation, adsorption and electrosorption process will increase the CIP removal efficiency. According to the results of this study, the use of MAC alone removed more than 70% of CIP and adding the EC process increased the efficiency by about 25%. Therefore, the predominant phenomenon in this process is adsorption, and with the addition of EC to the MAC process, which caused a 25% increase in efficiency. Therefore, in general, the adsorption processes play a major role in the elimination of CIP, and the effect of the chemical oxidation process is small [28,30].

In the EC-MAC process, the nanocomposite was simply separated by a magnet after the process and an increase in volume or sludge production was not observed. One sample of the MAC nanocomposites was analyzed by EDS after the EC-MAC process (Fig. 5a). As can be seen, the percentages of iron, carbon and oxygen were 48.65%, 13.90% and 37.45% and no Cu and Zn spectra were observed. This indicates that the dissolution of the electrode did not occur or the dissolution was so low that it was not detectable in the EDS test. Samples of the EC-MAC process effluent were also analyzed for electrode leaching and the amount of Zn and Cu entering the final effluent by atomic absorption spectrometry. The results of these experiments showed that Cu and Zn in the effluent were 41 and 135 $\mu\text{g/L}$, respectively. According to the Iranian Environmental Protection Agency, the amount of Cu and Zn in treated effluent, which is allowed to be discharged to surface water is 1 and 2 mg/L , respectively [39]. The values of Cu and Zn in effluent based on the United States Environmental Protection Agency are 0.25 and 1 mg/L , respectively [40]. Therefore, the amounts of these metals in the treated wastewater were much lower than the discharge standards.

The EC-MAC-NaCl process eliminated 95.5% of CIP after 60 min. Adding NaCl salt to the EC-MAC process increased the efficiency by 1%. This is because NaCl plays an electrolyte role and is usually used to improve the electrical conductivity of water or wastewater for better treatment. Electrical conductivity also affects Faradic yield, cell

voltage; as a result, it is expected to see an increase in process efficiency and a decrease in energy consumption in the EC reactor [41,42]. But, in this study, by adding NaCl salt, a large and green sludge was formed and corrosion was observed at the anode. The findings of the EDS analysis in the sludge from the EC-MAC-NaCl process (Fig. 5b) confirm the dissolution of the anode and the entry of Cu and Zn into the reaction reactor. According to previous studies, one of the disadvantages of adding salt to the EC reactor, despite its benefits, is the corrosion of the electrodes, which is consistent with the results of the present study [41]. It was found that adding NaCl salt to the EC-MAC process caused an ignorable increase in efficiency; furthermore, a high amount of non-recoverable sludge was produced. Hence, the current research was continued without adding salt to the EC-MAC process, because it is not economically and environmentally friendly.

The EC-MAC-PS process eliminated 98.9% of CIP after 60 min. By adding PS to the EC-MAC process, the removal efficiency increased by about 4.5%. This phenomenon may be due to an increase in the number of sulfate radicals due to the cathode reduction of the PS anions [according to Eqs. (1) and (2)] and the chemical oxidation process of CIP by sulfate radicals, which have a higher oxidation potential than hydroxyl radicals in the system. Thus, in addition to adsorption and electrosorption processes, oxidation with sulfate radicals also occurs, which increases removal efficiency [1,27].

Nevertheless, another phenomenon that happened during the EC-MAC-PS process was that some of the grayish sludge (less than the sludge produced in the EC-MAC-NaCl process) was produced, which was flocculated and separated by a magnet. This is owing to the presence of the MAC nanocomposites in the clot structure. The sludge from the EC-MAC-PS process was investigated by the EDS experiment (Fig. 5c). As can be seen, the amounts of Zn and Cu in the sludge were very low, which were not detectable. The sludge produced in the EC-MAC-PS process is a problem for the environment and needs to be treated, but in the EC-MAC process, the MAC nanocomposites are easily magnetically separable, regeneration and reusable. Also, the difference between the efficiency of EC-MAC-PS and EC-MAC was very low (about 4.5%). Therefore, the use of PS was neglected and the optimum conditions for the EC-MAC process were investigated.

3.3. Effect of key parameters on EC-MAC process

3.3.1. pH

The results of the effect of pH on the EC-MAC process have been shown in Fig. 6a. As indicated in the figure, there was an overall upward trend in the removal efficiency with increasing pH. The removal efficiencies of CIP at pHs: 3, 5, 7 and 9 after 60 min were 87, 94.21, 94.4 and 95.64%, respectively. The efficiency at acidic pH of 3 was the lowest, but the pHs of 5, 7 and 9 had a similar performance. Due to the proximity of the efficiencies, neutral pH 7 was selected as the optimum value. The pH of the CIP solution plays an important role in the adsorption and electrosorption processes because CIP exhibits different behaviors at different

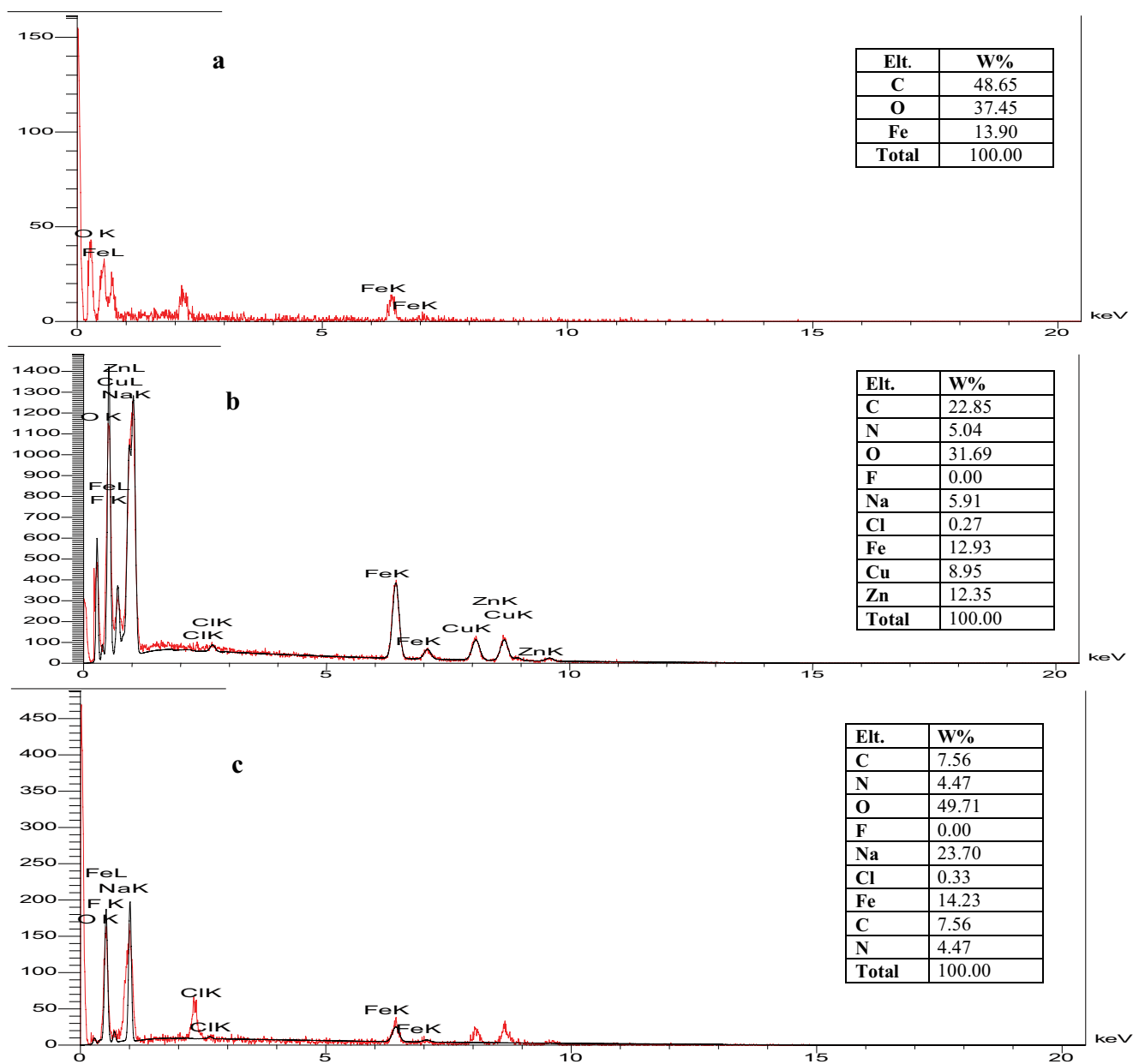


Fig. 5. Results of (a) EDS after EC-MAC process, (b) EDS after EC-MAC-NaCl process and (c) EDS after EC-MAC-PS process.

pH values. When pH is below 5.5, the CIP charge is positive (CIP^+), when pH is between 5.5 and 7.7, CIP behaves zwitterionically (CIP^z) and, when pH is greater than 7.7, CIP charge is neutral (CIP^0) [43,44]. The pH_{zpc} of the MAC nanocomposite was 6.4, hence, it was positive at $pH < 6.4$ and negative at $pH > 6.4$. Therefore, the MAC nanocomposite surface is positive and this phenomenon causes repulsive forces between the adsorbent and the antibiotic surface at acidic pH of 3, resulting in a decline in process efficiency. By increasing pH to 5.5, the MAC surface charge was positive and the charge of the antibiotic was neutral and zwitterionic, so the process efficiency increased slightly. In this research, the pH changes were also evaluated during the experiment, which showed that, after the final reaction time, the final pH

of the reactor reached the zwitterionic range (7–8); it should be noted that the highest removal rate also occurred in this area. In the study by Wu et al. [45], by using carbon aerogel as particle electrodes for decoloration of RBRX dye solution in a 3D-EC, pH of 5.1 was selected as the optimum value. Also, in the study by Pang et al. [22], in which paced activated carbon was used in the 3D-EC to remove organic pollutants, it was claimed that there was a similar trend for the optimum pH and the removal efficiency increased with raising pH.

3.3.2. MAC nanocomposite dose

In the previous studies with the 3D-EC process, mainly GAC has been used as a particle electrode, which eliminates

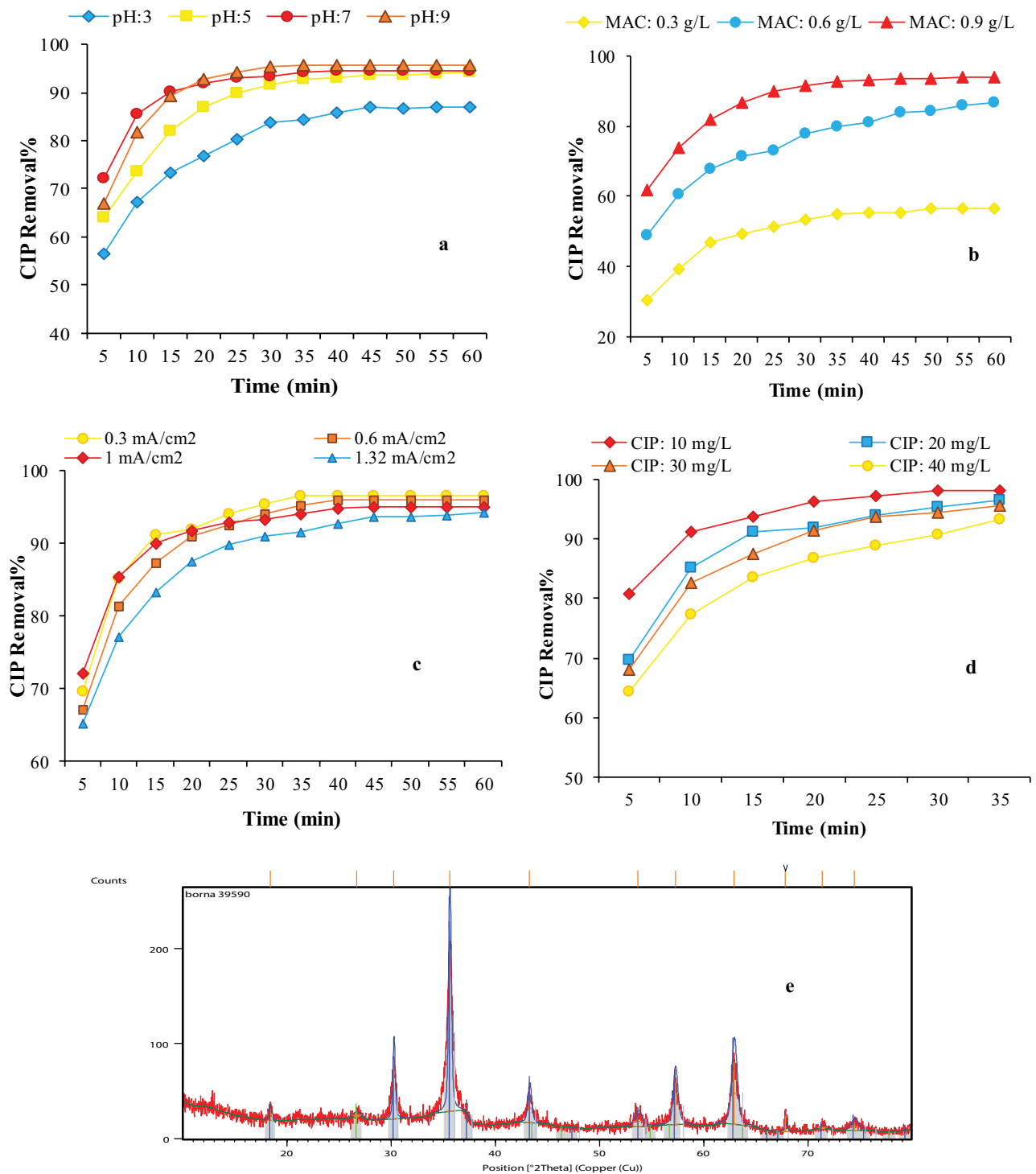


Fig. 6. The effect of (a) pH (experimental conditions: CIP = 20 mg/L, EC = 1 mA/cm², MAC = 0.9 g/L), (b) MAC dose (experimental conditions: CIP = 20 mg/L, EC = 1 mA/cm², pH = 7), (c) CD (experimental conditions: CIP = 20 mg/L, MAC = 0.9 g/L, pH = 7) and (d) initial CIP concentration (experimental conditions: CD = 0.3 mA/cm², MAC = 0.9 g/L, pH = 7) on EC-MAC process in CIP removal and (e) XRD results of MAC after process.

pollutants due to being exposed to the magnetic field by the adsorption and electrosorption processes. The amounts of GAC used in these studies were very significant between 50 and 110 g/L, which are not economically [18,20,23,24].

A plus factor of the synthesized MAC nanocomposite was that a much lower amount of it was needed and accordingly its performance was higher. Also, because of the magnetic properties of the MAC nanocomposite, they can be

easily separated and recovered in a short time. The results of the effect of different MAC nanocomposite doses on the EC-MAC process have been presented in Fig. 6b. As can be seen, the CIP removal efficiency increased with increasing the dose of the MAC nanocomposite. The removal efficiencies for different MAC nanocomposite doses: 0.3, 0.6 and 0.9 g/L after 60 min were 56.4%, 88.08% and 94.3%, respectively. An increase in the MAC nanocomposite dose leads to an increase in the adsorbent active sites, the increase of the number of particle electrodes and thus the increase of the useful surface of active electrodes, which perform adsorption and electrosorption [26,28]. The results obtained for the effect of the MAC nanocomposite dose are consistent with those of similar studies [25,26,28].

3.3.3. Current density

CD is one of the most important parameters in the 3D system because it not only produces hydroxyl radicals by hydrolysis of water and eliminates pollutants by the electrochemical oxidation process but also polarizes the MAC nanocomposites and creates particle electrodes. The creation of the particle electrodes increases the surface area of the electrodes and dominates the electrosorption process in addition to the adsorption process. Increasing the surface area of the electrodes also increases the production of hydroxyl radicals and consequently enhances the process efficiency [18,21,41]. On the other hand, an increase in CD increases energy consumption, as well as the cost of treatment, which makes the process uneconomically. Therefore, optimizing the CD and determining the optimum value is very important. The results of the influence of CD on the EC-MAC process have been shown in Fig. 6c. As can be seen, the CIP removal rates at the current densities of 0.3, 0.6, 1 and 1.32 mA/cm² were 96.6%, 96.11%, 95% and 94.25%, respectively. It was found that increasing CD had no effect on increasing the CIP removal efficiency and even slightly decreased the removal efficiency. The decrease in removal efficiency with increasing CD may be due to short-circuit current and bypass current, which occur with increasing CD [46]. Also, the high CD may lead to side reactions that have an adverse effect on the general CIP removal efficiency [24]. As mentioned above, the CD of 0.3 mA/cm² was chosen as the optimum value of the EC-MAC process. In other studies, using the 3D-EC process for the treatment of various pollutants, higher CD values (20–50 mA/cm²) have been reported as the optimal value [24,47–49]. Therefore, the CD value used in the present study was much lower than those claimed in other studies.

3.3.4. Initial CIP concentration

In general, the removal efficiency decreases with an increasing initial concentration of pollutants due to the increased contaminant load on the adsorption and oxidation processes occurring in 3D-EC. But, according to previous studies, this decrease in the 3D-EC process is relatively less than that in the adsorption and EC processes [30]. As shown in Fig. 6d, with MAC nanocomposite dose of 0.9 g/L at initial CIP concentrations of 10, 20, 30 and 40 mg/L, the removal efficiencies were 98.22%, 96.6%, 95.7%

Table 2
Adsorption kinetic models

Kinetic model	Equation
Pseudo-first-order	$q_t = q_e \times [1 - \exp(-k_f \times t)]$ (4)
Pseudo-second-order	$q_t = \frac{k_s \times q_e^2 \times t}{1 + (q_e \times k_s \times t)}$ (5)
Elovich	$q_t = \frac{1}{\beta} \ln(t + t_0) - \frac{1}{\beta} \ln(t_0)$ (6)
Avrami fractionary	$q_t = q_e \times [1 - \exp[-(k_{AV} \times t)]^{n_{AV}}]$ (7)

and 93.3%, respectively. As shown in the figure, the amount of the decrease in efficiency at high concentrations was very low, which is consistent with the results of other studies [16,20]. The main reason for the increase in removal efficiency with increasing CIP concentration is that, in theory, increasing the initial concentration of pollutants can reduce the mass transfer limitations resulting in an increase in pollutant removal efficiency [50].

3.3.5. Stability of MAC

A sample of the MAC nanocomposite was sent for the XRD analysis after undergoing the EC-MAC process. The results of this analysis have been indicated in Fig. 6f. The XRD patterns before and after the process were almost identical, indicating that no change in the structure of the MAC nanocomposite crystals had occurred. As a result, the synthesized nanocomposites had high chemical stability after being processed.

3.4. Kinetic study

The kinetic studies are fundamental in adsorption processes due to their significant role in designing full-scale removal plants. To find a rate-controlling step and to explore the mechanism involved in CIP adsorption, several kinetic models [Eqs. (4)–(7)] were considered as summarized in Table 2.

The experimental data were fitted with the studied kinetic models (Table 2) by using the Origin 8.5 program. The quality of fitting and also the validity of the models used in this work were ascertained by calculating the non-linear parameter (R^2_{adj}) by using Eqs. (8) and (9).

$$R^2 = \left[\frac{\sum_i^{n_p} (q_{i,exp} - \bar{q}_{exp})^2 - \sum_i^{n_p} (q_{i,exp} - q_{i,model})^2}{\sum_i^{n_p} (q_{i,exp} - \bar{q}_{exp})^2} \right] \quad (8)$$

$$R^2_{adj} = 1 - \left(1 - R^2 \right) \times \left(\frac{n_p - 1}{n_p - p - 1} \right) \quad (9)$$

The experimental data and the model predictions have been plotted in Fig. 7, and the kinetic parameters obtained have been presented in Table 3.

The results revealed that the Avrami fractionary and pseudo-second-order kinetic models fitted better the experimental results than the other models, indicating that the interaction between CIP and adsorption sites of MAC. As the pseudo-second-order kinetic model depicted that, with increasing MAC dose to CIP ratio, the ratio of the amount of CIP adsorbed at equilibrium to the initial amount of CIP increases, and the rate constant (k_s) also improves indicating faster adsorption of CIP.

3.5. Isotherm study

Batch adsorption experiments were carried out to obtain CIP concentrations in the liquid phase. Several adsorption models can be used to describe experimental data of adsorption isotherms. According to Table 4, the equilibrium data were modeled with the Freundlich, Langmuir,

Dubinin–Radushkevich, Temkin, Sips, Liu and Redlich–Peterson isotherms [Eqs. (10–16)].

This study aimed to find the best isotherm model that can correctly predict CIP removal and equilibrium liquid phase concentration. In order to fit the experimental and predicted values of adsorption capacity for plotting the isotherm curves, R^2_{adj} were calculated according to Eq. (9). The isotherm equations were fitted with the adsorption data at various MAC doses (Fig. 8). The parameters obtained in fitting the experimental data have been summarized in Table 5.

The results showed that, amongst the two-parameter models, the best data fit belonged to the Langmuir model, indicating the occurrence of adsorption by a homogenous monolayer process without any internal interactions among the adsorbed CIP ions on the MAC surface. Furthermore, the studied three-parameter isotherms indicated a good fit with the experimental results of CIP adsorption at various doses of MAC, based on the high R^2_{adj} values. Compared to the two-parameter models, the higher R^2_{adj} related to three-parameter

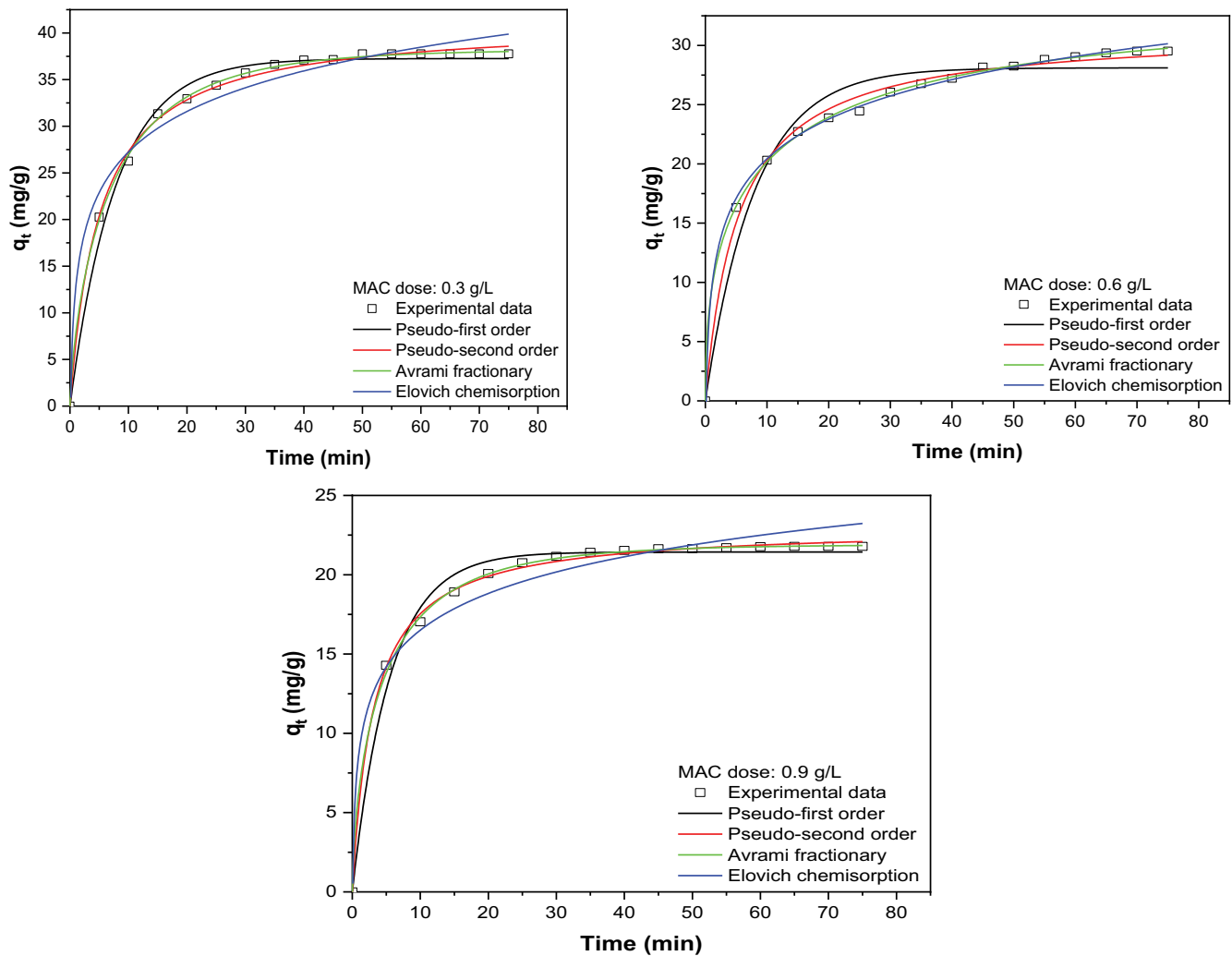


Fig. 7. Plots of different kinetic models for CIP adsorption onto MAC nanocomposite (solution pH = 7, initial CIP concentration = 20 mg/L).

Table 3
Values of kinetic parameters and correlation coefficients for the adsorption of CIP

Kinetic model	Constant parameter	MAC dose (g/L)		
		0.3	0.6	0.9
Pseudo-first-order	q_e	37.26 ± 0.32	28.1 ± 0.49	21.43 ± 0.19
	k_f	0.13 ± 0.006	0.12 ± 0.01	0.18 ± 0.01
	R^2_{adj}	0.991	0.95	0.986
Pseudo-second-order	q_e	41.21 ± 0.29	31.26 ± 0.34	23.01 ± 0.11
	k_s	0.005 ± 0.002	0.006 ± 0.004	0.014 ± 0.001
	R^2_{adj}	0.997	0.993	0.998
Elovich	A	48.25 ± 16.68	33.57 ± 0.38	46.78 ± 1.83
	B	0.16 ± 0.01	0.21 ± 0.005	0.29 ± 0.002
	R^2_{adj}	0.978	0.994	0.942
Avrami fractionary	q_e	38.21 ± 0.18	33.67 ± 0.77	21.91 ± 0.01
	k_{AV}	0.13 ± 0.003	0.09 ± 0.01	0.19 ± 0.0001
	n_{AV}	0.73 ± 0.02	0.46 ± 0.02	0.65 ± 0.003
	R^2_{adj}	0.999	0.999	0.996

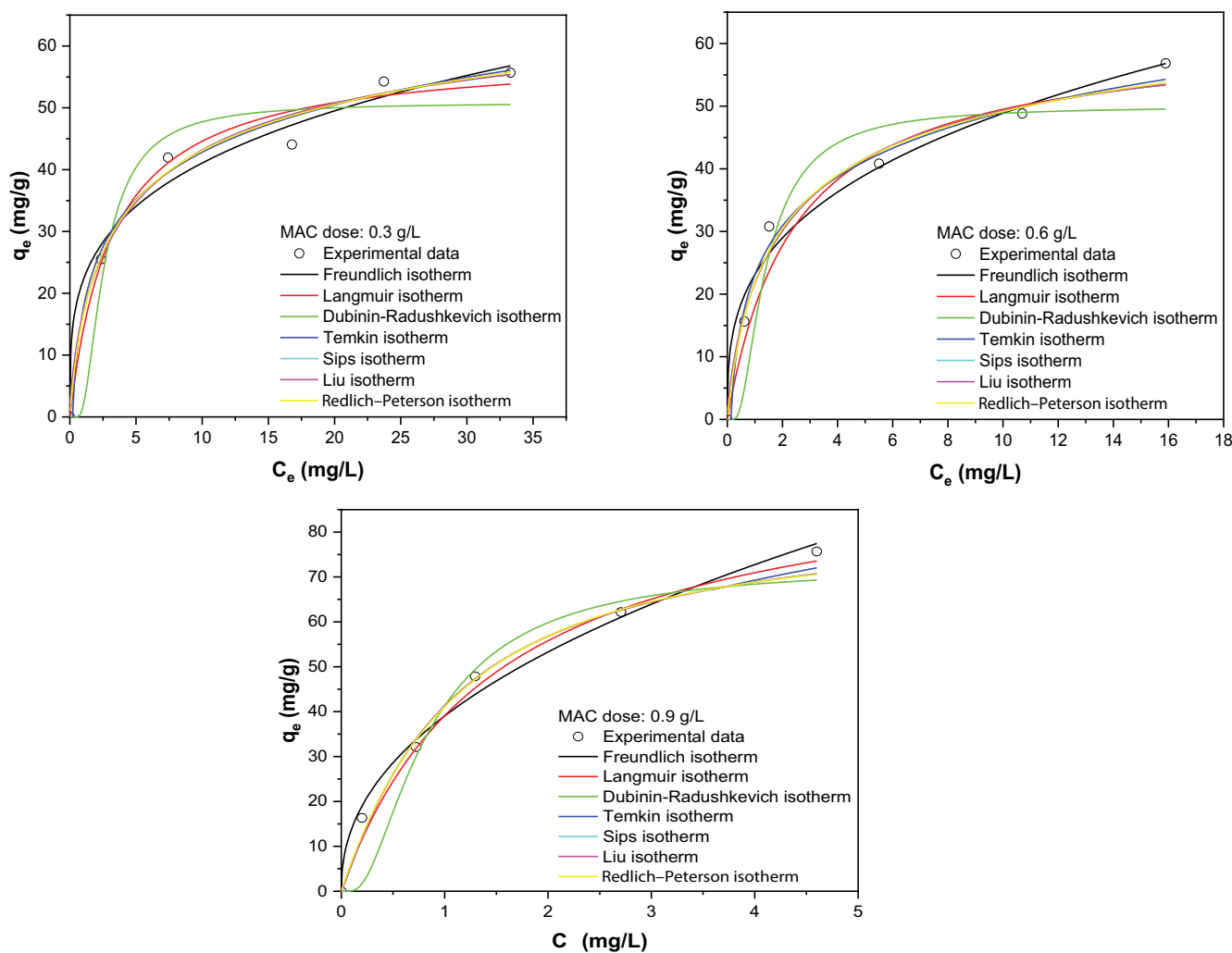


Fig. 8. Plots of isotherm models for CIP adsorption onto MAC nanocomposite.

Table 4
Adsorption isotherm models and parameters

Isotherm model	Equation
Freundlich	$q_e = K_F \times C_e^{1/n_F}$ (10)
Langmuir	$q_e = \frac{Q_{\max} \times K_L \times C_e}{1 + K_L \times C_e}$ (11)
Dubinin–Radushkevich	$q_e = Q_{\max} \exp(-K_{D-R} \varepsilon^2)$ (12)
Temkin	$q_e = \frac{RT}{b} \ln(A_T C_e)$ (13)
Sips	$q_e = \frac{Q_{\max} \times K_S \times C_e^{1/n_S}}{1 + K_S \times C_e^{1/n_S}}$ (14)
Liu	$q_e = \frac{Q_{\max} \times (K_g \times C_e)^{n_L}}{1 + (K_g \times C_e)^{n_L}}$ (15)
Redlich–Peterson	$q_e = \frac{K_{RP} \times C_e}{1 + a_{RP} \times C_e^G}$ (16)

Table 5
Values of isotherm parameters and correlation coefficients for the adsorption of CIP

Isotherm model	Constant parameter	MAC dose (g/L)		
		0.3	0.6	0.9
Freundlich	K_F	22.08 ± 2.68	23.13 ± 2.01	39.04 ± 1.52
	$1/n_F$	0.27 ± 0.04	0.32 ± 0.04	0.45 ± 0.03
	R^2_{adj}	0.978	0.979	0.991
Langmuir	Q_{\max}	59.09 ± 3.19	61.54 ± 0.27	97.39 ± 0.53
	K_L	0.31 ± 0.07	0.41 ± 0.007	0.67 ± 0.01
	R^2_{adj}	0.977	0.939	0.973
Dubinin–Radushkevich	Q_{\max}	50.84 ± 0.13	49.99 ± 0.17	72.52 ± 0.21
	K_{D-R}	1.13×10^{-6}	4.08×10^{-7}	1.9×10^{-7}
	R^2_{adj}	0.894	0.825	0.955
Temkin	A_T	4.86 ± 0.09	7.72 ± 0.35	8.58 ± 0.23
	B	11.02 ± 0.04	11.29 ± 0.13	19.59 ± 0.17
	R^2_{adj}	0.981	0.875	0.922
Sips	Q_{\max}	70.29 ± 0.56	66.78 ± 0.61	84.48 ± 1.23
	K_S	0.31 ± 0.002	0.48 ± 0.005	0.57 ± 0.03
	n_S	1.42 ± 0.02	1.31 ± 0.02	0.91 ± 0.02
Liu	R^2_{adj}	0.988	0.985	0.956
	Q_{\max}	70.29 ± 2.53	66.78 ± 2.44	84.48 ± 1.82
	K_g	0.19 ± 0.001	0.39 ± 0.001	0.96 ± 0.001
Redlich–Peterson	n_L	0.71 ± 0.001	0.76 ± 0.001	1.11 ± 0.001
	R^2_{adj}	0.999	0.99	0.99
	K_{RP}	28.91 ± 0.17	44.82 ± 0.19	68.75 ± 0.09
	a_{RP}	0.77 ± 0.007	1.05 ± 0.007	0.67 ± 0.001
	G	0.87 ± 0.001	0.89 ± 0.001	0.99 ± 0.001
	R^2_{adj}	0.999	0.999	0.999

isotherms illustrated that these models were more suitable than two-parameter models for the prediction of CIP adsorption by the MAC nanocomposite. As reported in Table 5, the theoretical maximum adsorption capacity (Q_{\max}) of the nanocomposite was obtained from all three-parameter models at various MAC doses close to the value obtained from the Langmuir model. Also, all the exponents of the three-parameter models were close to unity, signifying the adsorption of CIP onto MAC nanocomposite was a homogeneous process.

4. Conclusion

In this study, the MAC nanocomposite was synthesized and then used as particle electrodes in a 3D system in combination with PS. The characterization of the nanocomposite by related analyses indicated the formation of a proper nanoparticle structure and stability during the experiments. Among the EC-MAC and EC-MAC-PS processes, EC-MAC was selected as the appropriate process and optimum conditions for this process were determined. Moreover, the EC-MAC-PS method was excluded from further experiments because of producing unrecoverable sludge owing to using PS. Under the optimal conditions in the EC-MAC process, the CIP removal rate was 98.21% that is a very good efficiency. On the other hand, the MAC nanocomposite used in the EC-MAC process could easily be recovered and reused, which is one of the benefits of this process. Studies of isotherms and kinetics also showed that the Avrami fractional and pseudo-second-order kinetic models were the most consistent with the results of the present study and Q_{\max} obtained from the Langmuir isotherm model was found to be 97.39 mg/g. Overall, the present study had very good results in removing deodorants from aqueous solutions. However, it may have some limitations, such as the use of electricity and its cost, which would be minimized if optimization of the variable were done.

Acknowledgement

This research emanates from a doctoral dissertation and conducted at the Environmental Health Engineering Research Center and sponsored by the Vice-Chancellor for Research and Technology of Kerman University of Medical Sciences. The Ethic approval Cod is IR.KMU.REC.1398.447.

Symbols

q_{RP}	— Redlich–Peterson constants, mg/L
A_T	— Temkin constant, L/g
C_e	— Supernatant adsorbate concentration at the equilibrium, mg/L
g	— Redlich–Peterson exponent, dimensionless
k_{AV}	— Avrami kinetic constant, 1/min
K_{D-R}	— Adsorption energy, mol ² /kJ ²
K_F	— Freundlich equilibrium constant, mg/g
k_f	— Pseudo-first-order rate constant, 1/min
K_L	— Liu equilibrium constant, L/mg
K_L^S	— Langmuir equilibrium constant, L/mg
K_{RP}	— Redlich–Peterson constants, L/g
K_S	— Sips equilibrium constant, (mg/L) ^{-1/n}
k_S	— Pseudo-second-order rate constant, g/mg min

n_{AV}	— Fractional adsorption order
n_F	— Freundlich exponent, dimensionless
n_L	— Liu exponent, dimensionless
n_p	— Number of experiments performed
n_S	— Sips exponent
p	— Number of parameters of the fitted model
\bar{q}_{exp}	— Average of q experimentally measured
q_e	— Amount of adsorbate adsorbed at the equilibrium, mg/g
q_e	— Equilibrium adsorption capacity, mg/g
$q_{i,exp}$	— Value of q measured experimentally
$q_{i,model}$	— Value of q predicted by the fitted model
Q_{\max}	— Maximum adsorption capacity of the adsorbent, mg/g
q_t	— Amount of adsorbate adsorbed at time t , mg/g
R	— Universal gas constant, 8.314 J/mol K
t	— Contact time, min
T	— Absolute temperature, °K
α	— Initial adsorption rate, g/mg min
β	— Extent of surface coverage and the activation energy involved in chemisorption, g/mg
ε	— Polanyi potential

References

- [1] M. Malakootian, M. Ahmadian, Removal of ciprofloxacin from aqueous solution by electro-activated persulfate oxidation using aluminum electrodes, *Water Sci. Technol.*, 80 (2019) 587–596.
- [2] A. Nasiri, F. Tamaddon, M.H. Mosslemine, M. Faraji, A microwave assisted method to synthesize nanoCoFe₂O₄@methyl cellulose as a novel metal-organic framework for antibiotic degradation, *MethodsX*, 6 (2019) 1557–1563.
- [3] L. Chen, R. Ni, T. Yuan, Y. Gao, W. Kong, P. Zhang, Q. Yue, B. Gao, Effects of green synthesis, magnetization, and regeneration on ciprofloxacin removal by bimetallic nZVI/Cu composites and insights of degradation mechanism, *J. Hazard. Mater.*, 382 (2020) 121008.
- [4] L. Chen, T. Yuan, R. Ni, Q. Yue, B. Gao, Multivariate optimization of ciprofloxacin removal by polyvinylpyrrolidone stabilized NZVI/Cu bimetallic particles, *Chem. Eng. J.*, 365 (2019) 183–192.
- [5] S. Ganesan, M. Amirthalingam, P. Arivalagan, S. Govindan, S. Palanisamy, A.P. Lingassamy, V.K. Ponnusamy, Absolute removal of ciprofloxacin and its degraded byproducts in aqueous solution using an efficient electrochemical oxidation process coupled with adsorption treatment technique, *J. Environ. Manage.*, 245 (2019) 409–417.
- [6] H. Pourzamani, N. Mengelzadeh, H. Mohammadi, N. Niknam, B. Neamati, R. Rahimi, Comparison of electrochemical advanced oxidation processes for removal of ciprofloxacin from aqueous solutions, *Desal. Water Treat.*, 113 (2018) 307–318.
- [7] K. Luo, Y. Pang, Q. Yang, D. Wang, X. Li, L. Wang, M. Lei, J. Liu, Enhanced ciprofloxacin removal by sludge-derived biochar: effect of humic acid, *Chemosphere*, 231 (2019) 495–501.
- [8] M. Malakootian, A. Nasiri, A. Asadipour, E. Kargar, Facile and green synthesis of ZnFe₂O₄@CMC as a new magnetic nanophotocatalyst for ciprofloxacin degradation from aqueous media, *Process Saf. Environ. Prot.*, 129 (2019) 138–151.
- [9] C.A. Igwegbe, S. Ahmadi, S. Rahdar, A. Ramazani, A.R. Mol-lazehi, Efficiency comparison of advanced oxidation processes for ciprofloxacin removal from aqueous solutions: sonochemical, sono-nano-chemical and sono-nano-chemical/persulfate processes, *Environ. Eng. Res.*, 25 (2020) 178–185.
- [10] F. Yu, Y. Sun, M. Yang, J. Ma, Adsorption mechanism and effect of moisture contents on ciprofloxacin removal by three-dimensional porous graphene hydrogel, *J. Hazard. Mater.*, 374 (2019) 195–202.

- [11] C. Zheng, H. Zheng, C. Hu, Y. Wang, Y. Wang, C. Zhao, W. Ding, Q. Sun, Structural design of magnetic biosorbents for the removal of ciprofloxacin from water, *Bioresour. Technol.*, 296 (2020) 122288.
- [12] J.J.S. Alonso, N. El Kori, N. Melián-Martel, B. Del Río-Gamero, Removal of ciprofloxacin from seawater by reverse osmosis, *J. Environ. Manage.*, 217 (2018) 337–345.
- [13] P. Bhattacharya, D. Mukherjee, S. Dey, S. Ghosh, S. Banerjee, Development and performance evaluation of a novel CuO/TiO₂ ceramic ultrafiltration membrane for ciprofloxacin removal, *Mater. Chem. Phys.*, 229 (2019) 106–116.
- [14] M.T. Do, D.C. Stuckey, Fate and removal of ciprofloxacin in an anaerobic membrane bioreactor (AnMBR), *Bioresour. Technol.*, 289 (2019) 121683.
- [15] T.S. Khokhar, F.N. Memon, A.A. Memon, F. Durmaz, S. Memon, Q.K. Panhwar, S. Muneer, Removal of ciprofloxacin from aqueous solution using wheat bran as adsorbent, *Sep. Sci. Technol.*, 54 (2019) 1278–1288.
- [16] M.R. Samarghandi, S.A. Babae, M. Ahmadian, G. Asgari, F. Ghorbani Shahna, A. Poormohammadi, Performance catalytic ozonation over the carbosieve in the removal of toluene from waste air stream, *J. Res. Health Sci.*, 14 (2014) 227–32.
- [17] M.R. Heidari, R.S. Varma, M. Ahmadian, M. Pourkhosravani, S.N. Asadzadeh, P. Karimi, M. Khatami, Photo-Fenton like catalyst system: activated carbon/CoFe₂O₄ nanocomposite for reactive dye removal from textile wastewater, *Appl. Sci.*, 9 (2019) 963.
- [18] K.-W. Jung, M.-J. Hwang, D.-S. Park, K.-H. Ahn, Performance evaluation and optimization of a fluidized three-dimensional electrode reactor combining pre-exposed granular activated carbon as a moving particle electrode for greywater treatment, *Sep. Purif. Technol.*, 156 (2015) 414–423.
- [19] K.-W. Jung, M.-J. Hwang, D.-S. Park, K.-H. Ahn, Combining fluidized metal-impregnated granular activated carbon in three-dimensional electrocoagulation system: feasibility and optimization test of color and COD removal from real cotton textile wastewater, *Sep. Purif. Technol.*, 146 (2015) 154–167.
- [20] Z. Liu, F. Wang, Y. Li, T. Xu, S. Zhu, Continuous electrochemical oxidation of methyl orange waste water using a three-dimensional electrode reactor, *J. Environ. Sci.*, 23 (2011) S70–S73.
- [21] Y. Long, Y. Feng, X. Li, N. Suo, H. Chen, Z. Wang, Y. Yu, Removal of diclofenac by three-dimensional electro-Fenton-persulfate (3D electro-Fenton-PS), *Chemosphere*, 219 (2019) 1024–1031.
- [22] T. Pang, Y. Wang, H. Yang, T. Wang, W. Cai, Dynamic model of organic pollutant degradation in three dimensional packed bed electrode reactor, *Chemosphere*, 206 (2018) 107–114.
- [23] N.L. Pedersen, M. Nikbakht Fini, P.K. Molnar, J. Muff, Synergy of combined adsorption and electrochemical degradation of aqueous organics by granular activated carbon particulate electrodes, *Sep. Purif. Technol.*, 208 (2019) 51–58.
- [24] L. Wei, S. Guo, G. Yan, C. Chen, X. Jiang, Electrochemical pretreatment of heavy oil refinery wastewater using a three-dimensional electrode reactor, *Electrochim. Acta*, 55 (2010) 8615–8620.
- [25] J. Zhan, Z. Li, G. Yu, X. Pan, J. Wang, W. Zhu, X. Han, Y. Wang, Enhanced treatment of pharmaceutical wastewater by combining three-dimensional electrochemical process with ozonation to in situ regenerate granular activated carbon particle electrodes, *Sep. Purif. Technol.*, 208 (2019) 12–18.
- [26] Y. Zhang, Z. Chen, P. Wu, Y. Duan, L. Zhou, Y. Lai, F. Wang, S. Li, Three-dimensional heterogeneous electro-Fenton system with a novel catalytic particle electrode for bisphenol A removal, *J. Hazard. Mater.*, 393 (2020) 120448.
- [27] M. Ahmadian, M. Pirsaeheb, H. Janjani, H. Hossaini, Ultraviolet activated persulfate based AOP for MTBE decomposition in aqueous solution, *Desal. Water Treat.*, 161 (2019) 269–274.
- [28] H.-Z. Zhao, Y. Sun, L.-N. Xu, J.-R. Ni, Removal of acid orange 7 in simulated wastewater using a three-dimensional electrode reactor: removal mechanisms and dye degradation pathway, *Chemosphere*, 78 (2010) 46–51.
- [29] R. Shokooi, D. Nematollahi, M.R. Samarghandi, Gh. Azariana, Z. Latifi, Optimization of three-dimensional electrochemical process for degradation of methylene blue from aqueous environments using central composite design, *Environ. Technol. Innovation*, 18 (2020) 100711.
- [30] C. Zhang, Y. Jiang, Y. Li, Z. Hu, L. Zhou, M. Zhou, Three-dimensional electrochemical process for wastewater treatment: a general review, *Chem. Eng. J.*, 228 (2013) 455–467.
- [31] J. Choi, J. Chung, Evaluation of urea removal by persulfate with UV irradiation in an ultrapure water production system, *Water Res.*, 158 (2019) 411–416.
- [32] L. Liu, S. Lin, W. Zhang, U. Farooq, G. Shen, Kinetic and mechanistic investigations of the degradation of sulfachloropyridazine in heat-activated persulfate oxidation process, *Chem. Eng. J.*, 346 (2018) 515–524.
- [33] A. Seid-Mohammadi, G. Asgari, A. Poormohammadi, M. Ahmadian, H. Rezaeivahidian, Removal of phenol at high concentrations using UV/Persulfate from saline wastewater, *Desal. Water Treat.*, 57 (2016) 19988–19995.
- [34] T. Cai, Y. Liu, L. Wang, W. Dong, H. Chen, W. Zeng, X. Xia, G. Zeng, Activation of persulfate by photoexcited dye for antibiotic degradation: radical and nonradical reactions, *Chem. Eng. J.*, 375 (2019) 122070.
- [35] F. Nekouei, Sh. Nekouei, H. Noorizadeh, Enhanced adsorption and catalytic oxidation of ciprofloxacin by an Ag/AgCl@N-doped activated carbon composite, *J. Phys. Chem. Solids*, 114 (2018) 36–44.
- [36] M.K. Mohammadi Nodeh, S. Soltani, S. Shahabuddin, H. Rashidi Nodeh, H. Sereshti, Kinetic and thermodynamic study of magnetic polyaniline/graphene oxide based nanocomposites for ciprofloxacin removal from water, *J. Inorg. Organomet. Polym.*, 28 (2018) 1226–1234.
- [37] A. Gupta, A. Garg, Adsorption and oxidation of ciprofloxacin in a fixed bed column using activated sludge derived activated carbon, *J. Environ. Manage.*, 250 (2019) 109474.
- [38] T.M. Darweesh, M.J. Ahmed, Adsorption of ciprofloxacin and norfloxacin from aqueous solution onto granular activated carbon in fixed bed column, *Ecotoxicol. Environ. Saf.*, 138 (2017) 139–145.
- [39] Publications of the Environmental Protection Organization, Environmental Regulations and Standards of Effluent Reuse in Iran, Iran, Tehran, 2003.
- [40] M. Zeiner, T. Rezić, B. Šantek, Monitoring of Cu, Fe, Ni, and Zn in wastewater during treatment in a horizontal rotating tubular bioreactor, *Water Environ. Res.*, 82 (2010) 183–186.
- [41] I. Kabdaşlı, I. Arslan-Alaton, T. Ölmez-Hancı, O. Tünay, Electrocoagulation applications for industrial wastewaters: a critical review, *Environ. Technol.*, 1 (2012) 2–45.
- [42] A.C. Ndjomgoue-Yossa, C.P. Nansu-Njiki, I.M. Kengne, E. Ngamen, Effect of electrode material and supporting electrolyte on the treatment of water containing *Escherichia coli* by electrocoagulation, *Int. J. Environ. Sci. Technol.*, 12 (2015) 2103–2110.
- [43] X. Peng, F. Hu, F.L. Lam, Y. Wang, Z. Liu, H. Dai, Adsorption behavior and mechanisms of ciprofloxacin from aqueous solution by ordered mesoporous carbon and bamboo-based carbon, *J. Colloid Interface Sci.*, 460 (2015) 349–360.
- [44] S.T. Danaloglu, Ş.S. Bayazit, Ö. Kerkez, B.G. Alhogbi, M.A. Salam, Removal of ciprofloxacin from aqueous solution using humic acid and levulinic acid-coated Fe₃O₄ nanoparticles, *Chem. Eng. Res. Des.*, 123 (2017) 259–267.
- [45] X. Wu, X. Yang, D. Wu, R. Fu, Feasibility study of using carbon aerogel as particle electrodes for decoloration of RBX dye solution in a three-dimensional electrode reactor, *Chem. Eng. J.*, 138 (2008) 47–54.
- [46] W. He, Q. Ma, J. Wang, J. Yu, W. Bao, H. Ma, A. Amrane, Preparation of novel kaolin-based particle electrodes for treating methyl orange wastewater, *Appl. Clay Sci.*, 99 (2014) 178–186.
- [47] M.H. Zhou, L.C. Lei, Electrochemical regeneration of activated carbon loaded with p-nitrophenol in a fluidized electrochemical reactor, *Electrochim. Acta*, 51 (2006) 4489–4496.
- [48] F. Hussin, M.K. Aroua, M. Szlachta, Combined solar electrocoagulation and adsorption processes for Pb(II) removal from aqueous solution, *Chem. Eng. Process.*, 143 (2019) 107619.
- [49] X. Zhu, J. Ni, X. Xing, H. Li, Y. Jiang, Synergies between electrochemical oxidation and activated carbon adsorption in three-dimensional boron-doped diamond anode system, *Electrochim. Acta*, 56 (2011) 1270–1274.
- [50] B. Shen, X.-h. Wen, X. Huang, Enhanced removal performance of estril by a three-dimensional electrode reactor, *Chem. Eng. J.*, 327 (2017) 597–607.